

Article

Chiroptically Active Multi-Modal Calcium Carbonate-Based Nanocomposites

Fearghal C. Donnelly^{1,2}, Finn Purcell-Milton³, Eoin Caffrey⁴ , Lorenzo Branzi¹, Shelley Stafford¹ , Faisal Ali Alhammad¹, Olan Cleary¹, Munirah Ghariani¹, Vera Kuznetsova¹ and Yurii K. Gun'ko^{1,2,*} 

¹ School of Chemistry, Trinity College Dublin, D02 PN40 Dublin, Ireland; branzil@tcd.ie (L.B.); alhammaf@tcd.ie (F.A.A.)

² BiOrbic Bioeconomy SFI Research Centre, University College Dublin, D04 F438 Dublin, Ireland

³ Chemical & BioPharmaceutical Science, Technological University Dublin, Grangegorman, D07 H6K8 Dublin, Ireland

⁴ School of Physics, Trinity College Dublin, D02 PN40 Dublin, Ireland

* Correspondence: igounko@tcd.ie

Abstract: The development of multimodal nano- and micro-structures has become an increasingly popular area of research in recent years. In particular, the combination of two or more desirable properties within a single structure opens multiple opportunities from biomedicine, sensing, and catalysis, to a variety of optical applications. Here, for the first time, we report the synthesis and characterization of multimodal chiroptically active CaCO₃ nanocomposites. These composites have been prepared by a modified microemulsion method in the presence of an amino acid (cysteine). Following this, additional modalities have been introduced by loading the composites with luminescent nanoparticles or doping with Eu³⁺ ions. The luminescent composites have been produced by the incorporation of CuInZnS/ZnS or CdSe@ZnS/ZnS core/shell quantum dots, or via doping with trivalent europium. In this manner, we have produced chiroptically active composites with orange, green, and red luminescence. Overall, this work demonstrates the unique advantage and potential of our approach and new class of chiroptically active CaCO₃ nanocomposites, which display tunable functionality to specific requirements via the incorporation of desired ions, nanoparticles, and chirality of the structure.

Keywords: quantum dots; core-shell nanostructures; chiroptical activity; photoluminescence; calcium carbonate



Citation: Donnelly, F.C.; Purcell-Milton, F.; Caffrey, E.; Branzi, L.; Stafford, S.; Alhammad, F.A.; Cleary, O.; Ghariani, M.; Kuznetsova, V.; Gun'ko, Y.K. Chiroptically Active Multi-Modal Calcium Carbonate-Based Nanocomposites. *Nanomaterials* **2024**, *14*, 100. <https://doi.org/10.3390/nano14010100>

Academic Editor: Hui Huang

Received: 18 November 2023

Revised: 19 December 2023

Accepted: 27 December 2023

Published: 31 December 2023



Copyright: © 2023 by the authors. Licensee MDPI, Basel, Switzerland. This article is an open access article distributed under the terms and conditions of the Creative Commons Attribution (CC BY) license (<https://creativecommons.org/licenses/by/4.0/>).

1. Introduction

Calcium carbonate is amongst the oldest and most widely studied materials in existence. Naturally occurring as limestone, marble and chalk, it provides a major source of global CO₂ sequestration [1] as well as being an important biomineral responsible for a variety of animal and marine life functions. Industrially, it finds use in the construction industry, in the production of high gloss paper [2], and as white pigment in paint [3], as well as in various fields of biomedicine in both drug delivery and in calcium supplementation. It exists in three anhydrous forms, which are, in order of decreasing stability: calcite, aragonite, and vaterite, and possess three further hydrated forms: amorphous calcium carbonate (ACC), ikaite, and monohydrocalcite [4]. Additionally, we believe its biocompatibility and robust nature make it an ideal substrate to produce novel multi-modal materials.

A particularly interesting research area is the development of multimodal nano- and micro-composite structures [5–7] that can be specifically tailored to various applications including in sensing, photonics, catalysis, and drug delivery [7–11]. These structures have been demonstrated in a variety of materials including silica, various polymeric materials, and CaCO₃ offering the specific advantages of bioavailability in tandem with favorable optical properties. In the production of CaCO₃ composites, a variety of microemulsions

are frequently used, which generally rely on micelles to encapsulate the required moiety within the CaCO_3 matrix. These methods are highly effective and have found success, for example, in drug delivery. Oil-in-water (O/W) microemulsions, for example, have recently been used to encapsulate the anticancer drug doxorubicin (DOX) through a high-pressure homogenization (HPH) system and showed high selectivity with minimal associated toxicity in healthy tissue [12]. However, the CaCO_3 composites' applications are not limited to drug delivery: they have been recently used as vaccine adjuvants [13], while Liu et al. illustrated their potential for catalysis [14]. Nanocomposites based on Eu^{3+} -doped CaCO_3 have also been prepared using a traditional carbonation method and then calcined to obtain Eu^{3+} -doped CaO phosphors [15].

Chiral compounds, i.e., those that exist in two non-superimposable mirror-image forms known as enantiomers, are of exceptional importance to a variety of fields including chemistry, biology, and medicine. The enantioselectivity of chiral substances is highly useful in a variety of applications from enantiomeric separation to asymmetric catalysis as well as in biochemistry and other applications. In addition, many biomineralization processes are often heavily reliant on chirality, including the formation of various CaCO_3 -based structures.

Luminescent nanomaterials also possess an ever-increasing research interest. These materials find uses in several fields, from LEDs and photovoltaics to bioimaging and sensing. Two classes of luminescent nanomaterials, semiconductor quantum dots (QDs) and lanthanide-doped nanomaterials, present a particular interest. QDs are an important type of luminescent nanomaterials with a variety of controlled morphologies and associated luminescence properties [16]. Core-shell QDs, which are used in this work, involve the coating of a semiconductor with a shell of a second bandgap semiconductor, which allows the further tuning of their optical properties [17]. Lanthanide (e.g., Eu and Tb)-doped nanostructures are also a highly effective luminescent species and have been investigated extensively. It was demonstrated that the lanthanide doping of inorganic materials results in highly stable materials with large Stokes shifts, narrow emission peaks, and some of the longest photoluminescent lifetimes available [15,18–24]. QD-loaded inorganic structures have been used for numerous applications including but not limited to biosensing [25], as well as optical microresonators [26] and white light emitters [27]. Lanthanide-doped composites, meanwhile, have found applications in biological studies [28], upconversion [29], catalysis [30], and optoelectronics [21]. While Eu^{3+} doping of CaCO_3 has been studied and will be discussed below, the only few examples that exist of quantum dot loading into CaCO_3 composites have shown a preservation of their individual properties within the CaCO_3 matrix.

The main aim of this work is to develop a new class of chiroptically active multimodal CaCO_3 nanocomposites loaded with luminescent nanoparticles. These CaCO_3 -based composites have been prepared via a modified chiral ligand-assisted microemulsion approach. In addition, the composites have been loaded with a large variety of luminescent active components of remarkable importance in the literature. For this purpose, we focused our investigation on well-known luminophores such as cadmium selenide QDs shelled with ZnS (CdSe@ZnS/ZnS QDs) [31] and quaternary copper indium zinc sulfide passivated with ZnS shells (CuInZnS/ZnS QDs) [32–35] as well as Eu^{3+} ions resulting in new multimodal luminescent microstructures with a range of potential applications.

2. Experimental Section

2.1. Starting Materials

Calcium chloride dihydrate ($\text{CaCl}_2 \cdot 2\text{H}_2\text{O}$, $\geq 99.0\%$), sodium carbonate (Na_2CO_3 , $\geq 99.5\%$, ACS reagent, Barcelona, Spain), $\text{Eu}(\text{NO}_3)_3 \cdot 6\text{H}_2\text{O}$ (99.9%), cadmium acetate ($\geq 99.99\%$) polyvinylpyrrolidone (PVP) (MW 360,000), sodium dodecyl sulfate (SDS), copper iodide (CuI, 99.99%), indium acetate ($\text{In}(\text{OAc})_3$, 99.99%), 1-dodecanethiol (1-DDT, 98%), zinc stearate (technical grade), zinc acetate dehydrate (99.999%), 1-octadecene (ODE, $\geq 95\%$), trioctylphosphine (TOP, 97%), diphenylphosphine (DPP, 98%), oleic acid (OA,

$\geq 99\%$), cetyltrimethylammonium bromide (CTAB, 99%), L-cysteine (98%), L- ($\geq 99\%$), and D-proline (99%) were supplied by Sigma Aldrich, St. Louis, MO, USA (Merk, Darmstadt, Germany) and used without further purification. All solvents used were supplied by the Trinity College Dublin Hazardous Materials facility.

2.2. Synthesis of Chiroptically Active CaCO_3 Composites

SDS (0.5 g; 90 mmol), PVP (0.5 g; 34.7 mmol), and L-cysteine (0.6 g; 50 mmol) were added to 50 mL of Na_2CO_3 (0.1 M) and allowed to stir for 1 h. SDS (0.721 g; 50 mmol) was added to a 50 mL solution of CaCl_2 and stirred for 15 min before being added to the Na_2CO_3 solution. The resulting suspension was stirred for a further 1 h. The product was subsequently centrifuged and washed with Millipore water and ethanol before drying at 80 °C for 24 h. This process has resulted in yields in excess of 70%.

2.3. Synthesis of Colloidal CuInZnS/ZnS QDs

The quantum dots CuInZnS/ZnS were prepared according to previously published and modified by us procedures [35].

2.3.1. Synthesis of Colloidal CuInS QDs

A total of 0.2 mmol (0.0358 g) of CuI , 0.6 mmol (0.1168 g) of $\text{In}(\text{OAc})_3$, and 20 mL of 1-DDT were mixed in a 100 mL 3-neck flask. The flask was degassed for 30 min at 80 °C, and then the atmosphere was switched to argon. Under argon flux, the reaction temperature was increased to 215 °C, and held at this temperature for 10 min. Then, the heating mantle was removed and the reaction vessel was cooled to room temperature naturally. Without purification, the crude solution was ready for the synthesis of CuInZnS alloyed QDs.

2.3.2. Synthesis of Colloidal CuInZnS QDs

The Zn precursor solution was prepared by dissolving 0.6 mmol (0.3768 g) of zinc stearate in 8 mL of ODE. A total of 2 mL of TOP was injected into the reaction flask under argon gas. The mixture was heated to 100 °C until a clear precursor solution was obtained. Then, CuInZnS QDs were prepared through in situ cation exchange of the preformed CuInS QDs. The crude CuInS QD solution was degassed at 115 °C for 30 min to remove volatiles that were produced during the reaction. Then, the atmosphere was switched to argon and the temperature was set to 120 °C. When the temperature reached the target temperature, the zinc precursor solution was added drop-wise with a syringe that was set on a syringe pump over 30 min (injection rate = 20 mL/h) to the reaction vessel. When the injection was finished, the temperature was increased to 200 °C and maintained at that temperature for 90 min before cooling to RT. Without cleaning, the sample was ready for ZnS shell coating.

2.3.3. Synthesis of CuInZnS/ZnS QDs

A total of 4 mmol (2.53 g) of zinc stearate was dissolved in 10 mL of oleic acid, 10 mL of 1-DDT, and 20 mL of ODE. The mixture was degassed for 2 h at 30 °C under stirring and then the reaction vessel was flashed with argon. The crude CuInZnS QDs solution in the reaction vessel was degassed for 30 min at 120 °C to remove volatiles that produced during the reaction. Under an argon atmosphere, the temperature was increased to 220 °C. When the temperature reached 200 °C, the above precursor solution was injected into the reaction vessel with a syringe pump (the injection rate was ~4 mL/h for the volume of 40 mL), with the injection taking 10 h. After the injection, the solution was stirred for another 1 h at 220 °C. Then, the heating mantle was removed and the reaction vessel was cooled to RT naturally. Hot ethanol, toluene, and chloroform were used to purify the sample. The obtained clean CuInZnS/ZnS QDs were stored in chloroform in the fridge.

2.4. Synthesis of Colloidal CdSe@ZnS/ZnS QDs

CdSe@ZnS/ZnS QDs were prepared according to previously published and modified by us procedures [31].

A total of 0.7 mmol of Cd acetate and 1.7 mmol of Zn oxide were mixed with 3.5 mL of OA. This mixture was heated to 150 °C under an argon atmosphere. Then, 10 mL of 1-octadecene (ODE) was added into the reactor at that temperature, and the mixture was heated to 310 °C. An anionic stock solution was prepared by dissolving 2.5 mmol of Se and 2.5 mmol of S in 5 mL of TOP. Then, 2.0 (Se + S) mL of TOP was quickly injected into the above hot mixture and the reaction proceeded at that temperature for 10 min for the growth of CdSe@ZnS QDs. For producing CdSe@ZnS/ZnS QDs through an additional ZnS coating, 0.8 mmol of S dissolved in 2 mL of ODE was consecutively introduced into the above growth solution of CdSe@ZnS QDs at 310 °C, followed by a holding time of 12 min. Next, a Zn precursor stock solution, prepared by 1.43 mmol of zinc acetate dehydrate dissolved in a mixture of 1 mL of oleic acid and 4 mL of ODE, was injected at 310 °C, after which the temperature of the reaction became lowered to 270 °C. The sulfur stock solution was prepared from 4.8 mmol of S dissolved in 5 mL of TOP. Then, the sulfur precursor was introduced drop-wise and the additional ZnS shelling proceeded at 310 °C for 20 min. The resulting CdSe@ZnS and CdSe@ZnS/ZnS QDs were precipitated by adding excess ethanol and repeatedly washed with a solvent combination of hexane/ethanol (1:4 in volume ratio) by centrifugation, and the purified QDs were redispersed in chloroform.

2.5. Synthesis of Quantum Dot-Loaded CaCO₃ Composites

To produce quantum dot-loaded composites, the CdSe@ZnS/ZnS or CuInZnS/ZnS QDs (0.1 mL aliquot in chloroform) were added to 50 mL of Na₂CO₃ (0.1 M) solution along with SDS (0.5 g; 90 mmol), PVP (0.5 g; 34.7 mmol), and L-cysteine (0.6 g; 50 mmol). The mixture was stirred for 1 h. Then, SDS (0.721 g; 50 mmol) was added to a 50 mL solution of CaCl₂ and stirred for 15 min before being added to the Na₂CO₃ and QD solution above. The resulting suspension was stirred for a further 1 h. The precipitated product was subsequently centrifuged and washed with Millipore water and ethanol before drying at 80 °C for 24 h. This process resulted in yields of the product in excess of 70%.

2.6. Synthesis of Europium-Loaded CaCO₃ Composites

Europium calcium carbonate composites were prepared similarly to the QD-loaded composites above using Eu(NO₃)₃·6H₂O (0.223 g; 5 mmol) in 10 mL of Millipore water instead of QDs. The product was isolated by centrifugation, washed with Millipore water and ethanol and then dried at 80 °C for 24 h.

2.7. Instrumentation and Equipment

All diffuse reflectance (DR) UV-Vis spectroscopy measurements were acquired using a Perkin Elmer Lambda 1050 UV-Vis-NIR spectrophotometer (Perkin Elmer, Waltham, MA, USA) operating in transmission mode, with a 150 mm InGaAs integrating sphere. Samples were prepared for DR UV-Vis by drop-casting some of the colloidal suspension onto a VWR super premium microscope slide cut to size, followed by solvent evaporation using a hot plate at 100 °C. The spectra were recorded within the wavelength range of 200–400 nm.

Solid state diffuse reflectance circular dichroism (DRCD) absorption spectra were measured using a Jasco J-815 CD spectrometer (Jasco, Dublin, Ireland) with a DRCD-575 integrating sphere and BaSO₄ internal background in the wavelength range from 200 to 400 nm.

X-ray diffraction (XRD) patterns were recorded on a Bruker D2 Phaser 2nd Gen bench-top diffractometer (Bruker, Billerica, MA, USA) using Cu K α radiation ($\lambda = 1.5418 \text{ \AA}$) across a 2θ range of 15 to 55° with a step-size of 0.01° at 1 s/step using a zero-background Si sample holder. Unit cell parameters and crystallite size were determined by Rietveld refinement of the obtained patterns performed using FullProf v5.10 implemented in EXPGUI. The starting point for refinements was ($R - 3c$; $a = 4.99$; $c = 17.0615$).

Scanning electron microscopy (SEM) was carried out on a Zeiss Ultra Plus Scanning Electron Microscope (Zeiss, Jena, Germany) operating at 3.50 kV.

Transmission electron microscopy (TEM) was carried out on an FEI Titan Transmission Electron Microscope (FEI, Hillsboro, OR, USA) operating at 300 kV.

Focused ion beam (FIB) microscopy was carried out using a Zeiss AURIGA Focused Ion Beam Scanning Electron Microscope.

Mercury porosimetry was carried out using an Autocan-33 Porosimeter (Quantachrome, Hook, UK).

FT-IR transmission spectra were recorded on a Bruker Tensor II FT-IR spectrometer using a diamond UATR. The spectra were recorded in the range from 400 to 4000 cm^{-1} .

Photoluminescence (PL) spectra were recorded using a Horiba FluorMax-4 (Horiba, Kyoto, Japan) in phosphorimetry mode. Steady-state measurements were made using a 0.1 ms delay, a sample window of 25 ms, a flash count of 200, and an increment of 1 nm, using a solid-state powder. Excitation spectra were measured using excitation and emission slits of 2 nm and 2 nm while emission spectra were measured using excitation and emission slits of 3 nm and 3 nm. The powder samples were mounted on a solid sample holder, and instead, CdSe@ZnS/ZnS QDs and CuInZnS/ZnS QDs were characterized as colloidal solution in toluene.

Photoluminescence lifetime and time resolved emission spectra measurements were performed using a time-correlated single-photon counting (TCSPC) spectrometer (Fluorolog 3 Horiba Jobin Yvon) and a range of different semiconductor diode lasers (295 nm, 340 nm, and 393 nm “Nano LED”—HORIBA Jobin Yvon) with a pulse duration shorter than 1 ns for excitation. Eu³⁺ phosphorescence lifetime decay was determined using the decay by window mode; in addition, it was carried out using a flash delay of 0.05 ms, a flash count of 200, and excitation/emission slits of 3 nm and 3 nm.

EDS analysis was performed using an 80 mm² window Oxford Instrument (Abingdon-Thames, UK) Xmax EDX detector and working with an EHT of 15 KeV.

3. Results and Discussion

3.1. Synthesis of Multi-Modal CaCO₃ Nanocomposites

Two different types of nanoparticles have been used for incorporation into CaCO₃ composites, namely CuInZnS/ZnS QDs and CdSe@ZnS/ZnS QDs. Both possess core-shell structures with a ZnS shell and with CuInZnS and CdSe@ZnS cores, respectively. CdSe@ZnS means that CdSe is partially alloyed with ZnS, resulting in an improvement of QD optical properties. Both types of QDs have been synthesized using previously reported methods described in the Section 2 below. Cadmium selenide QDs are characterized by their narrow emission peak, which allows them a high color purity, which is ideal for application in QLED. Green-emitting cadmium selenide QDs have been produced according to the previous report from Lee and co-workers [31]. The authors observed superior optical properties as well as high stability for the CdSe QDs stabilized by a ZnS chemical composition gradient shell and a further coated with a second ZnS shell layer producing a giant 12.7 nm CdSe@ZnS/ZnS QDs. The role of large-band gap semiconductors such as ZnS is critical in obtaining a type-I band alignment and guaranteeing the consequent confinement of both the photo-generated electron and hole in the CdSe core, while minimizing the lattice mismatch. On the other hand, cadmium-free quaternary QDs such as copper indium zinc sulfide are of great interest due to their superior biocompatibility for the design of luminescent solar concentrators and white LED production [32–34]. Copper indium zinc sulfide QDs passivated with a zinc sulfide shell (CuInZnS/ZnS QDs) are produced using a protocol from Zhang and co-workers [35]. This approach is based on the isolation of a ternary copper indium sulfide core, the production of an alloyed quaternary core via ion exchange reaction in the presence of Zn²⁺, and finally ZnS passivation to produce a core-shell QDs. These specific CuInZnS/ZnS and CdSe@ZnS/ZnS QDs were chosen for their monodispersity and favorable optical properties as well as their broad range of applications. The TEM images of CdSe@ZnS/ZnS and CuInZnS/ZnS QDs used for encapsulation are shown in Figure 1. The morphology of the CdSe@ZnS/ZnS QDs is represented by spherical nanoparticles with an average size around 12 nm, which is characteristic of

the giant core–shell QDs structure. The CuInZnS/ZnS sample was dominated by small nanoparticles with an average diameter of around 3 nm. In both systems, the nanomaterial morphology is in good agreement with the reported methods [31,35].

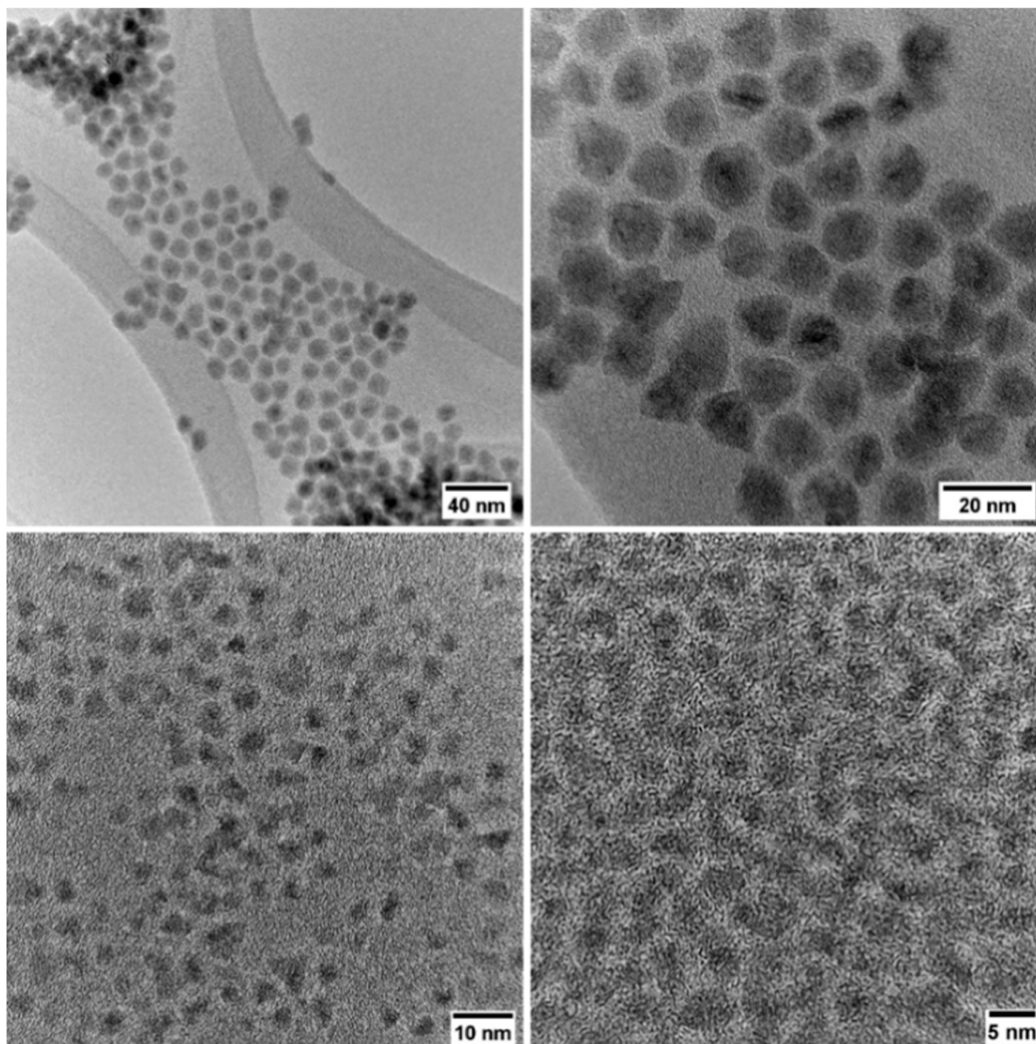


Figure 1. TEM images of CdSe@ZnS/ZnS QDs (top) and CuInZnS/ZnS QDs (bottom) that were used for the preparation of the calcium carbonate composites.

Chiroptically active luminescent CaCO_3 composites were produced using modified previously reported procedures [36,37], where complex micelles are formed through the combination of a polymer and surfactant, around which CaCO_3 structures are formed. Briefly, polyvinylpyrrolidone (PVP) and sodium dodecyl sulfate (SDS) are mixed, along with L-cysteine, in a Na_2CO_3 solution. To this, aliquots of luminescent (QDs or lanthanides) materials are added. Finally, a solution of CaCl_2 , which contains a further amount of SDS, is added to produce the composites with chiral, luminescent materials embedded within. A range of samples was produced (with the details given in the Section 2 below) and characterized using scanning electron microscopy (SEM), mercury porosimetry, focused ion beam (FIB) microscopy, X-ray diffractometric (XRD) studies, photoluminescence (PL), and diffuse reflectance circular dichroism (DRCD).

3.2. Structural Characterisation

Samples were studied via SEM with images given in Figure 2. Each sample demonstrated excellent monodispersity, with mean size distributions given in Supplementary Figure S1. The images show the formation of composites with high monodispersity and av-

erage diameters of $1.3 \pm 0.2 \mu\text{m}$ (CuInZnS/ZnS loaded) and $0.9 \pm 0.1 \mu\text{m}$ (CdSe@ZnS/ZnS loaded), and $3.0 \pm 0.5 \mu\text{m}$ for the Eu^{3+} -doped composites (Figure S1). Further micrographs of the CaCO_3 composites are shown in the Supporting Information file (Figures S2–S5). Interestingly, the addition of amino acids was shown to have no noticeable effect upon the diameter or distribution of the composites (SEM images of the achiral composites are shown in Figure S2).

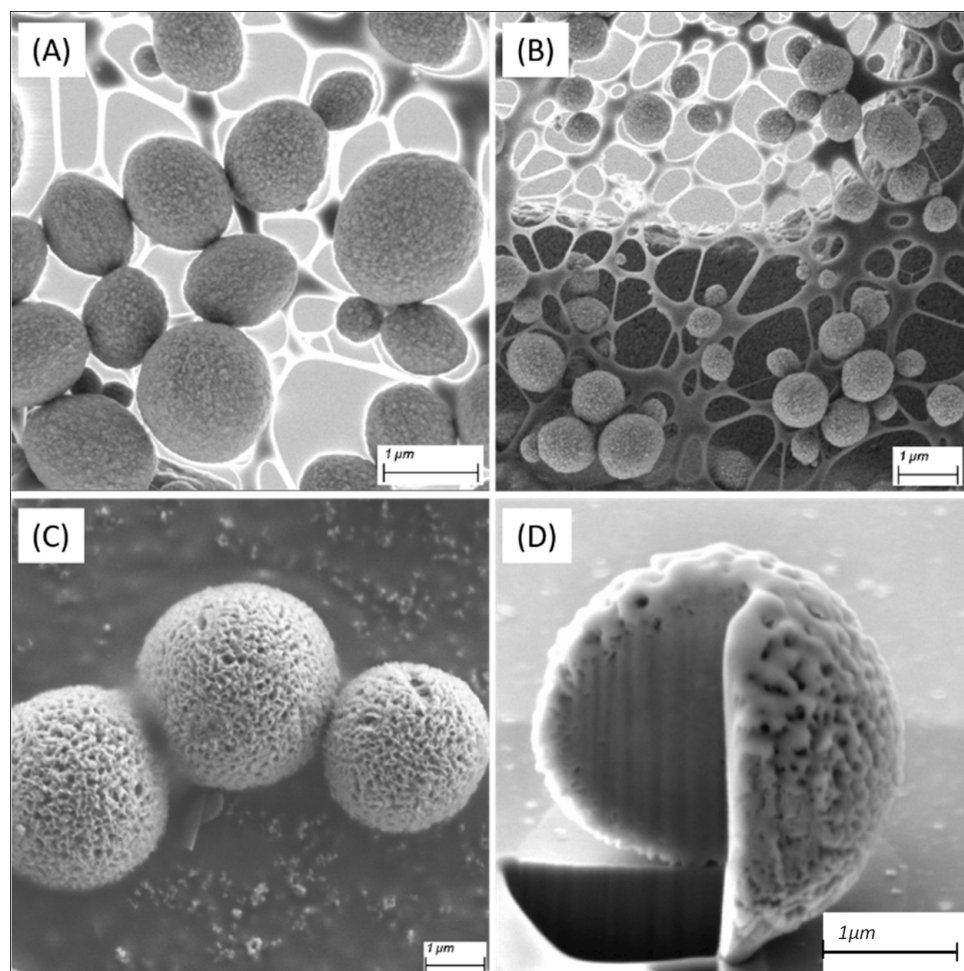


Figure 2. SEM images of the as-synthesized composites loaded with (A) CuInZnS/ZnS, (B) CdSe@ZnS/ZnS, and (C) doped with Eu^{3+} , and (D) FIB analysis showing a gallium milled cross section of a Eu^{3+} -doped CaCO_3 composite.

The various loaded composites showed no obvious morphological differences from each other apart from those doped with Eu^{3+} , which demonstrated both a marked increase in size and visible porosity (Figure 2C,D). This is to be expected, as while the QDs are simply loaded into the composites, Eu^{3+} has a high partition coefficient for calcite [38] and as such is readily incorporated into its matrix. This charge and size disparity, whereby two Eu^{3+} cations replace three Ca^{2+} cations, creates defects within the microsphere, which is likely the cause of the increased porosity and size. The porosity was analyzed using mercury porosimetry (see Supplementary Figure S6), giving two average size populations of 30 nm and 11 nm for undoped CaCO_3 while the mean diameter increased to 70 nm upon the addition of Eu^{3+} .

Focused ion beam (FIB) analysis (Figure 2D) showed that the composites formed were not hollow, while still being porous throughout. It is expected that some of this visible porosity was lost during the gallium-milling step of FIB, which causes an effect known as ‘curtaining’ whereby the mill pattern leads to the formation of large periodic strips down

the composites [39]. The formation of non-hollow porous composite microspheres is ideal for this work, as they provide a larger surface area within the microsphere to load the luminescent materials.

X-ray powder diffraction (XRD) analysis (Figure 3) showed that all three composite samples demonstrated the characteristic pattern of the CaCO_3 trigonal calcite phase (space group $R\text{-}3c$ n° 167) as reported for similar systems [40].

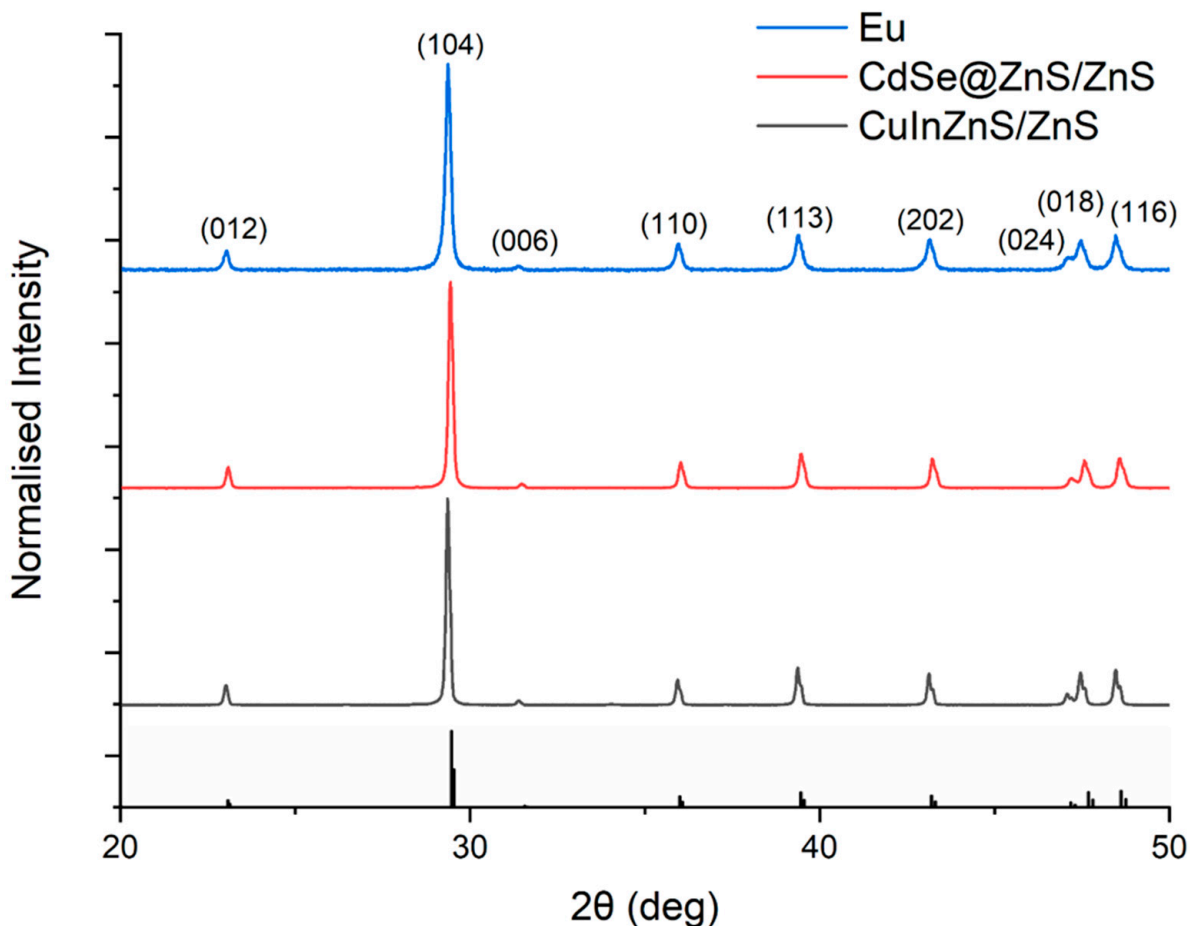


Figure 3. X-ray diffraction pattern of the (blue) Eu^{3+} -doped (red), CdSe@ZnS/ZnS , and (black) CuInZnS/ZnS -loaded composites showing the expected peaks for calcite. Reference pattern below: CaCO_3 calcite phase ICSD 18166.

The main diffractions are related to the (012), (104), (006), (110), (113), (202), (024), (018), and (116) planes of calcite and were observed at 23.31, 29.62, 31.63, 31.14, 39.51, 43.31, 47.24, 47.74, and 48.74 2θ degrees, respectively. The structure refinement (Figure S7) gives a unit cell of 4.9890 and 17.0689 Å for the a and c lattice parameters, respectively. An average crystallite size of 23 nm can be estimated using the Debye–Scherrer equation.

The XRD patterns of CdSe@ZnS/ZnS and CuInZnS/ZnS QDs are shown in Figure S7. The CdSe@ZnS/ZnS QDs XRD pattern (Figure S7A) shows a wurtzite hexagonal structure (space group $P63mc$ n° 186) as observed for similar CdSe QDs [41–43]. The diffractions can be assigned to the (100), (002), (101), (102), (2–10), (103), and (2–12) planes of the wurtzite lattice that were observed at 26.3, 27.7, 28.8, 38.6, 46.3, 49.5, 54.9 2θ degrees. The CuInZnS/ZnS QDs XRD pattern is shown in Figure S7B, where the nanoparticles are characterized by a cubic sphalerite (zincblende) structure (space group $F\text{-}43m$ n° 216). The main diffraction peaks can be assigned to the (111), (200), (220), and (311) planes that were observed at 48.5, 32.8, 47.6, and 56.0 2θ degrees, respectively. The small peak at 19.5 2θ degrees is often ascribed to a contribution from organic ligands [44]. In both cases, a

prominent shift of all the diffractions peaks toward higher angles compared to the CdSe and CuZn₂InS₄ phases is consistent with the incorporation of ZnS in the nanoparticles as well-documented for similar hetero-nanostructures produced by shelling or alloying with ZnS [35,45].

Due to the amount of QDs loaded in the CaCO₃ matrix and the intrinsic broadening of the QDs diffractions due to the nanocrystals' size, the XRD patterns of the composites produced with CdSe@ZnS/ZnS and CuInZnS/ZnS are completely dominated by the contribution originating from the CaCO₃ matrix. For this reason, energy dispersive x-ray spectroscopy (EDS) was used to estimate the loading of CaCO₃ composites. The EDS spectra of CdSe@ZnS/ZnS and CuInZnS/ZnS QDs are shown in Figure S8. The chemical composition analysis of CdSe@ZnS/ZnS QDs shows an atomic ratio of 1:40:14:23 for Cd, Zn, Se, and S respectively. Instead, CuInZnS/ZnS QDs are characterized by an atomic ratio of 1:1.5:20:23 for Cu:In:Zn:S, respectively. Both nanocrystals present a high content of zinc as also expected by their XRD patterns (Figure S8). The EDS spectra of the CaCO₃ composites (Figure S8) are mainly dominated by the peaks of the matrix, as can be appreciated by the intensity of the Ca K α peak at 3.69 KeV. The analysis of the Eu³⁺-doped CaCO₃ shows 3.9% of Eu³⁺, estimated by the intensity of the Eu L α (5.845 keV) and Eu M (1.131 keV) peaks. The spectra of the QDs-loaded composite show, with meaningful intensity, only peaks related to the main elements present in the nanocrystals such as zinc, sulfur, and selenium. An approximate estimation of the QD loading was performed considering the Zn L α (1.012 keV) and S K α (2.037 keV), which resulted in an estimated loading of 4.2% for CdSe@ZnS/ZnS QDs and 5.0% for CuInZnS/ZnS QDs.

3.3. Spectroscopic Characterisation

Diffuse reflectance circular dichroism (DRCD) and UV-Vis spectroscopy were carried out on all materials, as illustrated in Figure 4. A solid-state analytical technique was chosen owing to the poor solubility of CaCO₃, which limits the effectiveness of analysis in solution. In DRCD, an integrating sphere coated with BaSO₄ is used to allow the precise solid-state analysis of chiral compounds. BaSO₄ was the chosen material for coating due to its highly reflective properties; it can reflect light evenly across a wide range of wavelengths. The UV-Vis band positions at 205 and 265 nm correspond to CaCO₃ [46]. The circular dichroism data of the four samples illustrate the chiral nature of each. There is a dominating CD band that is portrayed by all three spectra in the UV region. This band appears at 220 nm, 230 nm, and 260 nm for the CuInZnS/ZnS QDs, CdSe@ZnS/ZnS QDs, and the Eu³⁺-loaded CaCO₃ composites, respectively. All the CaCO₃ composites show a strong absorption in the UV range due to the matrix, and no absorption in the visible range can be appreciated. This is likely due to the modest level of QD loading. L-cysteine is a well-known chiral amino acid, which is often used to impart chirality to nanoparticles [47]. It should be noted that the CD signal differs significantly from the CD spectrum of L-cysteine (See Supplementary Figure S9), proving that the signal is not due to free cysteine. Instead, what is observed is a lack of the Cotton effects, which is typical for chiral molecules (whereby there is a change in optical rotation in the region of maximum absorption). A potential rationalization of this phenomenon is that the amino acid is bonded to CaCO₃ in such a way that its conformational freedom is highly restricted. In this scenario, the amino acid is incapable of rotating in such a way as to produce Cotton effects, i.e., the 'switching' of the chiral signal at the point of maximum absorbance.

FT-IR was also carried out to confirm the presence of cysteine in the composites and is shown in Supplementary Figure S10. Briefly, the main contribution to the FTIR spectra can be related to the calcite matrix. Indeed, the strong broad peak centered around 1450 cm⁻¹ is related to the asymmetric C-O stretching ν_3 band, and two narrow peaks at 870 and 710 cm⁻¹ are related to CO₃ ν_2 plane deformation and O-C-C bending ν_4 , respectively; the latter is characteristic of crystalline CaCO₃ [48]. The peaks around 3000 cm⁻¹ correspond to the CH₃ and CH₂ stretching modes and a broad band related to the COOH functional groups of cysteine [49].

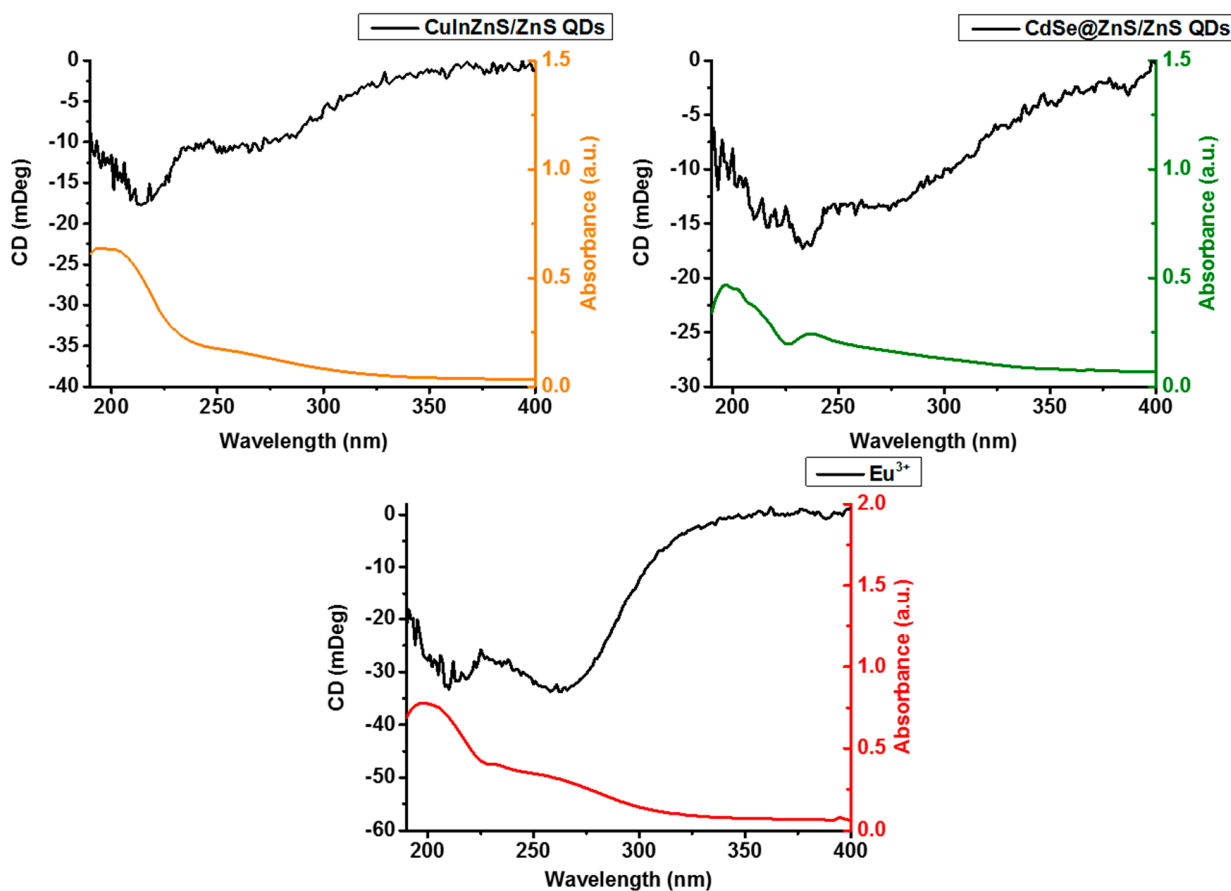


Figure 4. Diffuse reflectance circular dichroism (DRCD) spectroscopy of the CaCO_3 composites. The black line represents CD spectra while the colored spectra represent the UV-Vis absorbance spectra of the materials.

3.4. Investigation of Photoluminescence in Eu^{3+} -Doped and QD-Loaded CaCO_3 Composites

Following the proceeding work, we carried out characterization of the luminescent properties of the Eu^{3+} -doped and the CuInZnS/ZnS QD- and CdSe@ZnS/ZnS QD-loaded composites, with the results shown in Figures 5 and 6, respectively.

The excitation photoluminescence spectra (PLEx) and the emission photoluminescence spectra (PLEm) of Eu^{3+} -doped CaCO_3 composites are shown in Figure 5 with the characteristic peaks as has been reported in our previous work and other literature sources [18]. Emission spectra were recorded from 560 nm to 720 nm using an excitation of 393 nm corresponding to ${}^7\text{F}_0-{}^5\text{L}_6$ and using an excitation wavelength of 270 nm corresponding to the absorption energy of the $\text{O}^{2-}/\text{Eu}^{3+}$ charge transfer band (CTB) [50]. Upon excitation at 393 nm, the emission spectrum (Figure 5) is composed of narrow emission lines centered at 579, 590, 614, 650, and 699 nm. They correspond to the ${}^5\text{D}_0-{}^7\text{F}_j$ ($j = 0, 1, 2, 3, 4$) transitions characteristic of the Eu^{3+} ions. The strongest peak is located at 614 nm, which can be related to the ${}^5\text{D}_0-{}^7\text{F}_2$ transition [50]. As common for similar systems [50], the two strongest peaks at 589 and 614 nm correspond to the ${}^5\text{D}_0-{}^7\text{F}_1$ and ${}^5\text{D}_0-{}^7\text{F}_2$ transitions, respectively. While the former is magnetic dipole-allowed and local symmetry-independent, the latter is an induced dipole transition and is strongly dependent on local symmetry.

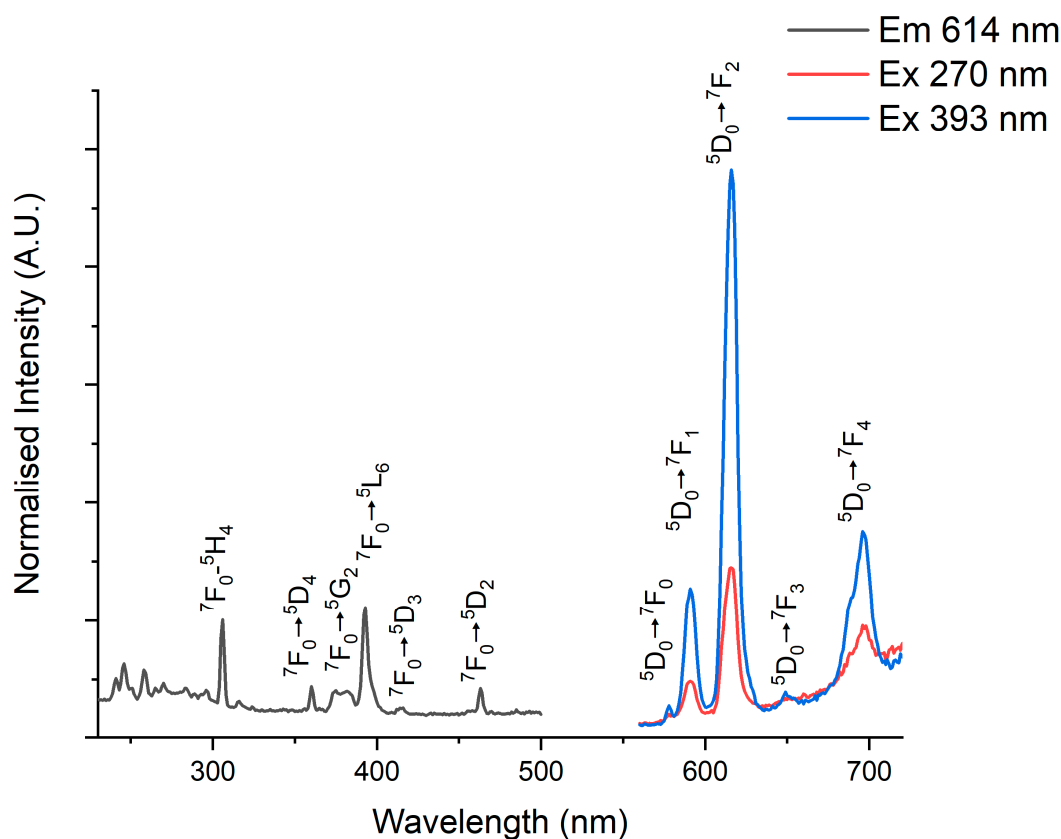


Figure 5. Emission and excitation photoluminescence spectra of Eu^{3+} -doped CaCO_3 composites. Emission was measured using excitation at 270 nm and 393 nm, while excitation was measured using the 614 nm peak, which corresponds to the ${}^5\text{D}_0$ - ${}^7\text{F}_2$ transition.

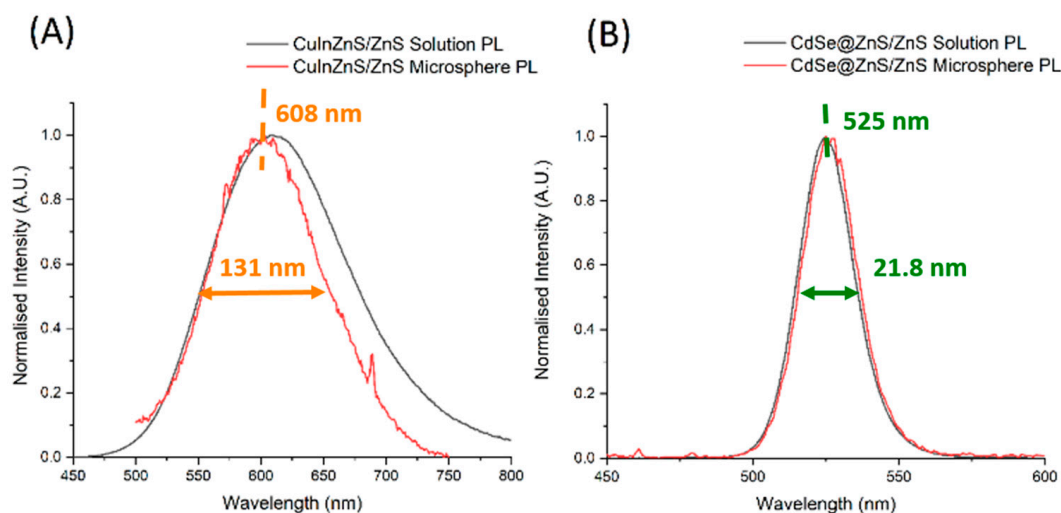


Figure 6. Photoluminescent emission spectra of CuInZnS/ZnS (A) and CdSe@ZnS/ZnS (B) in solution and loaded into CaCO_3 composites.

Photoluminescent spectra of the QD-loaded samples compared to the original QD PL in toluene solution are shown in Figure 6. The CuInZnS/ZnS QD-loaded CaCO_3 demonstrated a broad emission profile with a full width at half maximum (FWHM) of 131 nm, peaking at 608 nm, which is indicative of this type of QD. Indeed, as reported by Castro et al., copper indium sulfide quantum dots are characterized by a large Stokes shift and FWHM in the order of hundreds of nanometers [51]. Due to their detailed analysis

of the origin of these optical features, the authors established that multiple intraband defects are involved in the radiative recombination via a donor–acceptor recombination mechanism. CdSe@ZnS/ZnS QD-loaded CaCO₃ showed a much sharper emission peak with an FWHM of 21.8 nm centered on 525 nm, which is well-documented for the emission of II–VI QDs, which is dominated by a band-to-band recombination mechanism [31].

When comparing the QD-loaded composites' PL to the PL of the original solutions, no significant red-shifting of the peak position is noticeable upon incorporation inside the CaCO₃ lattice for either sample, with the CuInZnS/ZnS in fact showing a minor blue shift. The absence of red-shifting indicates that both QDs were incorporated singly throughout the composites' structures and have avoided aggregation, which leads to strong red-shifting in the PL emission peak.

To further characterize the effects of composite loading upon the PL emission, the fluorescence lifetime was measured for each sample and compared to the original QD prior to incorporation (Table 1). CdSe@ZnS/ZnS QD in toluene solution showed a monoexponential decay with a lifetime of 14.4 ns; this value is in agreement with the observation reports on CdSe QDs shelled with ZnS [31,52]. The photoluminescent decay of CuInZnS/ZnS QDs were fit with a triexponential decay to take into account multiple types of defects that can contribute to the emission via a donor–acceptor recombination mechanism [51]. An average lifetime of 434 ns is estimated; average lifetime values in the order of few hundreds of nanoseconds are in line with the behavior of copper indium sulfide and zinc alloyed systems [53,54]. In both cases, the QDs displayed a minor decrease in PL lifetime after the incorporation in CaCO₃. CdSe@ZnS/ZnS QDs showed a decrease from an average time of 14 ns in solution to 6.4 ns in the CaCO₃, while CuInZnS/ZnS QDs showed a more significant decrease from 434 to 295 ns. Therefore, this indicates increased de-excitation, which can be explained via binding with cysteine molecules, which passivate the QD surface less effectively than the original ligands. This may also be related to defects at the QDs–CaCO₃ interface, likely due to lattice mismatching that can act as a new pathway for non-radiative recombination process, causing the observed reduction in lifetimes.

Table 1. Fluorescence lifetimes of QDs and QD-loaded composites.

Sample	T ₁ (ns)	A ₁ (a.u)	T ₂ (ns)	A ₂ (a.u)	T ₃ (ns)	A ₃ (a.u)	T _{ave} (ns)
CdSe@ZnS/ZnS QDs solution	14.4	-	-	-	-	-	-
CdSe@ZnS/ZnS QDs in CaCO ₃	6.4	-	-	-	-	-	-
CuInZnS/ZnS QDs solution	163	0.2287	335	0.5854	1080	0.1859	434
CuInZnS/ZnS QDs in CaCO ₃	71.5	0.142	335	0.8502	8.32	0.0074	295

For Eu³⁺-doped calcium carbonate composites, the measured lifetime values were fitted using biexponential decay and were found to be T₁ = 0.398 ms and T₂ = 1.488 ms, with T_{ave} = 0.635 ms using the excitation wavelength of 393 nm. The results are well in line with previous reports for Eu³⁺-doped calcium carbonate composites [18].

4. Conclusions

Thus, we have successfully prepared several types of new multimodal CaCO₃ nanocomposites. Initially, achiral CaCO₃ composites were synthesized using a modified reported procedure. Their subsequent use of amino acids imparted a unique chiroptical activity and CD signal to these structures for the first time. The CD activity itself presents a significant research interest, as its extension to the upper wavelengths seems to point to a type of

‘chiral scattering’ or ‘chiral complexation’. Using this observation, the occurrence of chiral encapsulation can be determined using CD spectroscopy.

These composites have subsequently been used to encapsulate various luminescent materials. The encapsulation of CdSe@ZnS/ZnS and CuInZnS/ZnS QDs imparted green and orange fluorescence, respectively, whilst Eu³⁺ was used to produce red photoluminescent doped CaCO₃, with these emission spectra studied in detail.

With the addition of this functionality, we have demonstrated the intrinsic multimodal nature of this new class of chiral composites via the loading of specific ions or nanoparticles. Overall, this work is an important example of the new approaches to multimodal chiroptically active materials, which are expected to attract much attention and find a range of applications in the coming years.

Supplementary Materials: The following supporting information can be downloaded at: <https://www.mdpi.com/article/10.3390/nano14010100/s1>, Figure S1. Size distributions of (A) CuInZnS/ZnS (B) CdSe@ZnS/ZnS loaded and (C) Eu³⁺ doped microspheres where $N = 160, 150$ and 175 , respectively. Figure S2. Achiral CaCO₃ composites. Figure S3. SEM images of CaCO₃ composites loaded with CuInZnS:ZnS QDs. Figure S4. SEM images of CaCO₃ composites loaded with CdSe@ZnS/ZnS QDs. Figure S5. SEM images of Eu³⁺ doped CaCO₃ composites. Figure S6. Mercury porosimetry measurements of doped and undoped CaCO₃ composites. Figure S7. (A) XRD pattern of CdSe@ZnS/ZnS QDs, reference pattern: CdSe wurtzite phase (black) ICSD 415784 and ZnS wurtzite phase (red) 67453. (B) XRD pattern of CuInZnS/ZnS QDs, reference patterns: CuZn₂InS₄ sphalerite phase (black) and ZnS sphalerite phase (red). The asterisk marks the residual contribution from organic ligands. Figure S8. EDS spectra of CdSe@ZnS/ZnS, CuInZnS/ZnS QDs and the different CaCO₃ composites. Figure S9. CD spectrum of L-cysteine in water. Figure S10. FT-IR spectra of the composites loaded with (A) CuInZnS/ZnS, (B) CdSe@ZnS/ZnS and (C) doped with Eu³⁺ illustrating the presence of cysteine as evidenced by its characteristic peaks at 3000 cm⁻¹.

Author Contributions: Conceptualization, Y.K.G.; Methodology, F.C.D., E.C., S.S., V.K. and Y.K.G.; Validation, F.C.D. and M.G.; Formal analysis, F.P.-M., S.S., F.A.A., O.C., M.G. and V.K.; Investigation, F.C.D., F.P.-M., E.C., L.B., F.A.A. and O.C.; Writing—original draft, F.C.D., F.P.-M. and L.B.; Writing—review & editing, L.B., V.K. and Y.K.G.; Supervision, Y.K.G.; Funding acquisition, Y.K.G. All authors have read and agreed to the published version of the manuscript.

Funding: This research was funded by the Science Foundation Ireland, SFI (project: SFI-20/FFP-A/8904) and the SFI Bioeconomy Research Centre, Biorbic (project: SFI 16/RC/3889).

Data Availability Statement: Data are available in section “MDPI Research Data Policies” at <https://www.mdpi.com/ethics> (accessed on 26 December 2023).

Conflicts of Interest: The authors declare no conflicts of interest.

References

1. Doney, S.C.; Fabry, V.J.; Feely, R.A.; Kleypas, J.A. Ocean Acidification: The Other CO₂ Problem. *Annu. Rev. Mar. Sci.* **2009**, *1*, 169–192. [[CrossRef](#)] [[PubMed](#)]
2. Wang, S.; Ihalainen, P.; Järnström, J.; Peltonen, J. The Effect of Base Paper and Coating Method on the Surface Roughness of Pigment Coatings. *J. Dispers. Sci. Technol.* **2009**, *30*, 961–968. [[CrossRef](#)]
3. Karakaş, F.; Vaziri Hassas, B.; Çelik, M.S. Effect of precipitated calcium carbonate additions on waterborne paints at different pigment volume concentrations. *Prog. Org. Coat.* **2015**, *83*, 64–70. [[CrossRef](#)]
4. Boyjoo, Y.; Pareek, V.K.; Liu, J. Synthesis of micro and nano-sized calcium carbonate particles and their applications. *J. Mater. Chem. A* **2014**, *2*, 14270–14288. [[CrossRef](#)]
5. Kim, D.-H.; Li, W.; Chen, J.; Zhang, Z.; Green, R.M.; Huang, S.; Larson, A.C. Multimodal Imaging of Nanocomposite Microspheres for Transcatheter Intra-Arterial Drug Delivery to Liver Tumors. *Sci. Rep.* **2016**, *6*, 29653. [[CrossRef](#)] [[PubMed](#)]
6. John, R.; Nguyen, F.T.; Kolbeck, K.J.; Chaney, E.J.; Marjanovic, M.; Suslick, K.S.; Boppart, S.A. Targeted Multifunctional Multimodal Protein-Shell Microspheres as Cancer Imaging Contrast Agents. *Mol. Imaging Biol.* **2012**, *14*, 17–24. [[CrossRef](#)] [[PubMed](#)]
7. Sukhorukov, G.B.; Volodkin, D.V.; Günther, A.M.; Petrov, A.I.; Shenoy, D.B.; Möhwald, H. Porous calcium carbonate microparticles as templates for encapsulation of bioactive compounds. *J. Mater. Chem.* **2004**, *14*, 2073–2081. [[CrossRef](#)]
8. Zhao, Y.; Feng, J.; Hong, L.; Li, Y.; Wang, C.; Ye, S. Simple surface-assisted formation of palladium nanoparticles on polystyrene microspheres and their application in catalysis. *Inorg. Chem. Front.* **2018**, *5*, 1133–1138. [[CrossRef](#)]

9. Lundin Johnson, M.; Noreland, D.; Gane, P.; Schoelkopf, J.; Ridgway, C.; Millqvist Fureby, A. Porous calcium carbonate as a carrier material to increase the dissolution rate of poorly soluble flavouring compounds. *Food Funct.* **2017**, *8*, 1627–1640. [[CrossRef](#)]
10. Singh, R.; Lillard, J.W. Nanoparticle-based targeted drug delivery. *Exp. Mol. Pathol.* **2009**, *86*, 215–223. [[CrossRef](#)]
11. Yu, J.; Yu, J.C.; Zhang, L.; Wang, X.; Wu, L. Facile fabrication and characterization of hierarchically porous calcium carbonate microspheres. *Chem. Commun.* **2004**, *21*, 2414–2415. [[CrossRef](#)] [[PubMed](#)]
12. Shafiu Kamba, A.; Ismail, M.; Tengku Ibrahim, T.A.; Zakaria, Z.A. A pH-sensitive, biobased calcium carbonate aragonite nanocrystal as a novel anticancer delivery system. *Biomed. Res. Int.* **2013**, *2013*, 587451. [[CrossRef](#)] [[PubMed](#)]
13. Jia, J.; Liu, Q.; Yang, T.; Wang, L.; Ma, G. Facile fabrication of varisized calcium carbonate microspheres as vaccine adjuvants. *J. Mater. Chem. B* **2017**, *5*, 1611–1623. [[CrossRef](#)] [[PubMed](#)]
14. Liu, Y.; Shen, W.; Cui, H. Combined Transition-Metal/Enzyme Dual Catalytic System for Highly Intensive Glow-Type Chemiluminescence-Functionalized CaCO₃ Microspheres. *Anal. Chem.* **2019**, *91*, 10614–10621. [[CrossRef](#)] [[PubMed](#)]
15. Zhao, Q.; Qian, B.; Wang, Y.; Duan, T.; Zou, H.; Song, Y.; Sheng, Y. Facile synthesis of CaO:Eu³⁺ and comparative study on the luminescence properties of CaO:Eu³⁺ and CaCO₃:Eu³⁺. *J. Lumin.* **2022**, *241*, 118491. [[CrossRef](#)]
16. Sarkar, S.; Banerjee, D.; Ghorai, U.K.; Das, N.S.; Chattopadhyay, K.K. Size dependent photoluminescence property of hydrothermally synthesized crystalline carbon quantum dots. *J. Lumin.* **2016**, *178*, 314–323. [[CrossRef](#)]
17. Elliott, S.D.; Moloney, M.P.; Gun'ko, Y.K. Chiral shells and achiral cores in CdS quantum dots. *Nano Lett.* **2008**, *8*, 2452–2457. [[CrossRef](#)]
18. Donnelly, F.C.; Purcell-Milton, F.; Dunne, P.W.; Rulikowska, A.; Alguacil, V.; Gun'ko, Y.K. Luminescent calcium carbonate micro 'bow ties'. *Mater. Today Commun.* **2019**, *20*, 100590. [[CrossRef](#)]
19. Al Rifai, S.A.; Kulnitskiy, B.A. Microstructural and optical properties of europium-doped zinc oxide nanowires. *J. Phys. Chem. Solids* **2013**, *74*, 1733–1738. [[CrossRef](#)]
20. Escudero, A.; Moretti, E.; Ocana, M. Synthesis and luminescence of uniform europium-doped bismuth fluoride and bismuth oxyfluoride particles with different morphologies. *CrystEngComm* **2014**, *16*, 3274–3283. [[CrossRef](#)]
21. Martínez-Castro, E.; García-Sevillano, J.; Cussó, F.; Ocaña, M. Template-free synthesis and luminescent properties of hollow Ln:YOF (Ln = Eu or Er+Yb) microspheres. *J. Alloys Compd.* **2015**, *619*, 44–51. [[CrossRef](#)]
22. Candelario-Flores, L.; Reyes-Miranda, J.; Oliva, J.; Medina-Velazquez, D.Y.; Barrón Meza, M.A.; Garfias-García, E.; Gárrido Hernández, A.; García, C.R. Maximizing the red emission of CaCO₃:Eu³⁺ phosphors by using a Taguchi L9 orthogonal design. *J. Phys. Chem. Solids* **2021**, *154*, 110091. [[CrossRef](#)]
23. Wang, H.; Wang, Y.; Zhao, Q.; Zhou, X.; Zou, H.; Song, Y.; Sheng, Y. The preparation, structure and luminescent properties of Mg–CaCO₃:Eu³⁺ phosphors. *CrystEngComm* **2021**, *23*, 1517–1528. [[CrossRef](#)]
24. Chen, F.; Zhang, Y.; Feng, W.; Zhao, D.; Ruan, M.; Zhang, Q. Morphology control and luminescent properties of Eu/Tb-doped calcium carbonate nanoparticles using natural limestone. *J. Lumin.* **2021**, *238*, 118259. [[CrossRef](#)]
25. Cai, W.-Y.; Feng, L.-D.; Liu, S.-H.; Zhu, J.-J. Hemoglobin-CdTe-CaCO₃@Polyelectrolytes 3D Architecture: Fabrication, Characterization, and Application in Biosensing. *Adv. Funct. Mater.* **2008**, *18*, 3127–3136. [[CrossRef](#)]
26. Hanley, C.A.; McCarthy, J.E.; Purcell-Milton, F.; Gerard, V.; McCloskey, D.; Donegan, J.; Rakovich, Y.P.; Gun'ko, Y.K. Preparation and Investigation of Quantum-Dot-Loaded Hollow Polymer Microspheres. *J. Phys. Chem. C* **2013**, *117*, 24527–24536. [[CrossRef](#)]
27. Wu, Y.; Zhang, H.; Pan, A.; Wang, Q.; Zhang, Y.; Zhou, G.; He, L. White-Light-Emitting Melamine-Formaldehyde Microspheres through Polymer-Mediated Aggregation and Encapsulation of Graphene Quantum Dots. *Adv. Sci. (Weinh. Baden-Wuertt. Ger.)* **2018**, *6*, 1801432. [[CrossRef](#)]
28. Kuan, C.-Y.; Lin, Y.-Y.; Yang, I.-H.; Chen, C.-Y.; Chi, C.-Y.; Li, C.-H.; Chen, Z.-Y.; Lin, L.-Z.; Yang, C.-C.; Lin, F.-H. The Synthesis of Europium-Doped Calcium Carbonate by an Eco-Method as Free Radical Generator Under Low-Intensity Ultrasonic Irradiation for Body Sculpture. *Front. Bioeng. Biotechnol.* **2021**, *9*, 765630. [[CrossRef](#)]
29. Fernandez-Bravo, A.; Yao, K.; Barnard, E.S.; Borys, N.J.; Levy, E.S.; Tian, B.; Tajon, C.A.; Moretti, L.; Altoe, M.V.; Aloni, S.; et al. Continuous-wave upconverting nanoparticle microlasers. *Nat. Nanotechnol.* **2018**, *13*, 572–577. [[CrossRef](#)]
30. Moran, C.E.; Hale, G.D.; Halas, N.J. Synthesis and Characterization of Lanthanide-Doped Silica Microspheres. *Langmuir* **2001**, *17*, 8376–8379. [[CrossRef](#)]
31. Lee, K.H.; Lee, J.H.; Kang, H.D.; Park, B.; Kwon, Y.; Ko, H.; Lee, C.; Lee, J.; Yang, H. Over 40 cd/A efficient green quantum dot electroluminescent device comprising uniquely large-sized quantum dots. *ACS Nano* **2014**, *8*, 4893–4901. [[CrossRef](#)] [[PubMed](#)]
32. Zhong, H.; Bai, Z.; Zou, B. Tuning the Luminescence Properties of Colloidal I–III–VI Semiconductor Nanocrystals for Optoelectronics and Biotechnology Applications. *J. Phys. Chem. Lett.* **2012**, *3*, 3167–3175. [[CrossRef](#)] [[PubMed](#)]
33. Yang, L.; Zhang, S.; Xu, B.; Jiang, J.; Cai, B.; Lv, X.; Zou, Y.; Fan, Z.; Yang, H.; Zeng, H. I–III–VI Quantum Dots and Derivatives: Design, Synthesis, and Properties for Light-Emitting Diodes. *Nano Lett.* **2023**, *23*, 2443–2453. [[CrossRef](#)] [[PubMed](#)]
34. Dharmo, L.; Carulli, F.; Nickl, P.; Wegner, K.D.; Hodoroaba, V.-D.; Würth, C.; Brovelli, S.; Resch-Genger, U. Efficient Luminescent Solar Concentrators Based on Environmentally Friendly Cd-Free Ternary AIS/ZnS Quantum Dots. *Adv. Opt. Mater.* **2021**, *9*, 2100587. [[CrossRef](#)]
35. Zhang, A.; Dong, C.; Li, L.; Yin, J.; Liu, H.; Huang, X.; Ren, J. Non-blinking (Zn)CuInS/ZnS Quantum Dots Prepared by In Situ Interfacial Alloying Approach. *Sci. Rep.* **2015**, *5*, 15227. [[CrossRef](#)] [[PubMed](#)]
36. Zhao, L.; Wang, J. Biomimetic synthesis of hollow microspheres of calcium carbonate crystals in the presence of polymer and surfactant. *Colloids Surf. A Physicochem. Eng. Asp.* **2012**, *393*, 139–143. [[CrossRef](#)]

37. Shen, Q.; Wei, H.; Wang, L.; Zhou, Y.; Zhao, Y.; Zhang, Z.; Wang, D.; Xu, G.; Xu, D. Crystallization and Aggregation Behaviors of Calcium Carbonate in the Presence of Poly(vinylpyrrolidone) and Sodium Dodecyl Sulfate. *J. Phys. Chem. B* **2005**, *109*, 18342–18347. [[CrossRef](#)]
38. Voigt, M.; Mavromatis, V.; Oelkers, E.H. The experimental determination of REE partition coefficients in the water-calcite system. *Chem. Geol.* **2017**, *462*, 30–43. [[CrossRef](#)]
39. Loeber, T.H.; Laegel, B.; Wolff, S.; Schuff, S.; Balle, F.; Beck, T.; Eifler, D.; Fitschen, J.H.; Steidl, G. Reducing curtaining effects in FIB/SEM applications by a goniometer stage and an image processing method. *J. Vac. Sci. Technol. B* **2017**, *35*, 06GK01. [[CrossRef](#)]
40. Donnelly, F.C.; Purcell-Milton, F.; Framont, V.; Cleary, O.; Dunne, P.W.; Gun'ko, Y.K. Synthesis of CaCO₃ nano- and micro-particles by dry ice carbonation. *Chem. Commun.* **2017**, *53*, 6657–6660. [[CrossRef](#)]
41. Talapin, D.V.; Nelson, J.H.; Shevchenko, E.V.; Aloni, S.; Sadtler, B.; Alivisatos, A.P. Seeded Growth of Highly Luminescent CdSe/CdS Nanoheterostructures with Rod and Tetrapod Morphologies. *Nano Lett.* **2007**, *7*, 2951–2959. [[CrossRef](#)] [[PubMed](#)]
42. Li, J.; Zheng, H.; Zheng, Z.; Rong, H.; Zeng, Z.; Zeng, H. Synthesis of CdSe and CdSe/ZnS Quantum Dots with Tunable Crystal Structure and Photoluminescent Properties. *Nanomaterials* **2022**, *12*, 2969. [[CrossRef](#)]
43. Chauhan, H.; Kumar, Y.; Deka, S. New synthesis of two-dimensional CdSe/CdS core@shell dot-in-hexagonal platelet nanoheterostructures with interesting optical properties. *Nanoscale* **2014**, *6*, 10347–10354. [[CrossRef](#)] [[PubMed](#)]
44. Guillemeneu, L.; Lermusiaux, L.; Davidson, P.; Hubley, A.; Pierini, S.; Pierucci, D.; Patriarche, G.; Canut, B.; Lhuillier, E.; Mahler, B.; et al. Critical Role of Water on the Synthesis and Gelling of γ -In₂S₃ Nanoribbons with a Giant Aspect Ratio. *Chem. Mater.* **2022**, *34*, 9270–9281. [[CrossRef](#)]
45. Hao, J.; Liu, H.; Miao, J.; Lu, R.; Zhou, Z.; Zhao, B.; Xie, B.; Cheng, J.; Wang, K.; Delville, M.-H. A facile route to synthesize CdSe/ZnS thick-shell quantum dots with precisely controlled green emission properties: Towards QDs based LED applications. *Sci. Rep.* **2019**, *9*, 12048. [[CrossRef](#)] [[PubMed](#)]
46. Al Omari, M.M.; Rashid, I.S.; Qinna, N.A.; Jaber, A.M.; Badwan, A.A. Calcium Carbonate. *Profiles Drug Subst. Excip. Relat. Methodol.* **2016**, *41*, 31–132. [[CrossRef](#)]
47. Cho, N.H.; Guerrero-Martínez, A.; Ma, J.; Bals, S.; Kotov, N.A.; Liz-Marzán, L.M.; Nam, K.T. Bioinspired chiral inorganic nanomaterials. *Nat. Rev. Bioeng.* **2023**, *1*, 88–106. [[CrossRef](#)]
48. Rodríguez-Blanco, J.D.; Shaw, S.; Benning, L.G. The kinetics and mechanisms of amorphous calcium carbonate (ACC) crystallization to calcite, viavaterite. *Nanoscale* **2011**, *3*, 265–271. [[CrossRef](#)]
49. Basik, M.; Mobin, M.; Shoeb, M. Cysteine-silver-gold Nanocomposite as potential stable green corrosion inhibitor for mild steel under acidic condition. *Sci. Rep.* **2020**, *10*, 279. [[CrossRef](#)]
50. Blanco-Gutierrez, V.; Demourgues, A.; Jubera, V.; Gaudon, M. Eu(III)/Eu(II)-doped (Ca_{0.7}Sr_{0.3})CO₃ phosphors with vaterite/calcite/aragonite forms as shock/temperature detectors. *J. Mater. Chem. C* **2014**, *2*, 9969–9977. [[CrossRef](#)]
51. Castro, S.L.; Bailey, S.G.; Raffaele, R.P.; Banger, K.K.; Hepp, A.F. Synthesis and Characterization of Colloidal CuInS₂ Nanoparticles from a Molecular Single-Source Precursor. *J. Phys. Chem. B* **2004**, *108*, 12429–12435. [[CrossRef](#)]
52. Ratnesh, R.K.; Mehata, M.S. Investigation of biocompatible and protein sensitive highly luminescent quantum dots/nanocrystals of CdSe, CdSe/ZnS and CdSe/CdS. *Spectrochim. Acta Part A Mol. Biomol. Spectrosc.* **2017**, *179*, 201–210. [[CrossRef](#)] [[PubMed](#)]
53. Chen, Y.; Li, S.; Huang, L.; Pan, D. Green and Facile Synthesis of Water-Soluble Cu–In–S/ZnS Core/Shell Quantum Dots. *Inorg. Chem.* **2013**, *52*, 7819–7821. [[CrossRef](#)] [[PubMed](#)]
54. Zang, H.; Li, H.; Makarov, N.S.; Velizhanin, K.A.; Wu, K.; Park, Y.-S.; Klimov, V.I. Thick-Shell CuInS₂/ZnS Quantum Dots with Suppressed “Blinking” and Narrow Single-Particle Emission Line Widths. *Nano Lett.* **2017**, *17*, 1787–1795. [[CrossRef](#)]

Disclaimer/Publisher’s Note: The statements, opinions and data contained in all publications are solely those of the individual author(s) and contributor(s) and not of MDPI and/or the editor(s). MDPI and/or the editor(s) disclaim responsibility for any injury to people or property resulting from any ideas, methods, instructions or products referred to in the content.